ACS OMEGA

Open Access

http://pubs.acs.org/journal/acsodf

Article

Online Estimation of Combustion Oxygen Content with an Image-Augmented Soft Sensor Using Imbalanced Flame Images

Shuang Gao, Angpeng Liu, Yuxin Jiang, and Yi Liu*

Cite This: *ACS Omega* 2023, 8, 40657−40664

Read Online

ACCESS | Metrics & More | Article Recommendations

ABSTRACT: High-accuracy oxygen content measurement and control is one key to improving combustion efficiency and economic efficiency. The soft measurement technique of the oxygen content based on flame images is promising. However, image feature acquisition at different oxygen contents and image generation under unbalanced conditions are still challenging. To relieve this dilemma, a new generative-based regression model is developed. It not only learns the potential vectors but also captures flame features well to generate virtually high-quality-labeled flame images. The training data sets can be augmented, thus saving a lot of data collection experiments. Subsequently, a convolutional-based regression model is constructed to estimate the oxygen content using the augmented flame images directly. The designed method generates informative flame images and obtains more accurate oxygen content estimation results than several common methods.

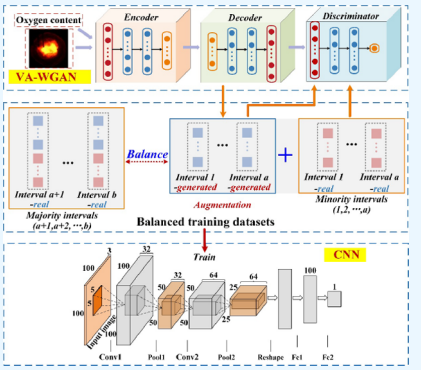

1. INTRODUCTION

Furnace combustion flames generated by the convective heat transfer between fuel and gas are used to heat the process fluid. The suitable oxygen content is extremely important for combustion during operation. A too high oxygen content would result in significant oxygen consumption and energy loss as well as increased emissions of nitrogen oxides and other pollutants. In contrast, a too low oxygen content would lead to incomplete chemical reactions, accelerated fouling of the equipment, and an impact on the final yield. The combustion oxygen content is closely related to the efficiency of the entire heat exchange process as well as the operational safety of the equipment. High-precision and real-time oxygen content measurement technology is an important support to accomplish combustion oxygen content control. However, the measurement accuracy of oxygen content analyzers is susceptible by the location of the sampling point and the measurement lag.[1] Moreover, the costs of the purchase and maintenance are high. Poor measurement performance limits the effectiveness of oxygen concentration control and is not conducive to improving efficiency.

Recently, the rapid development of deep learning and image processing methods has brought great changes to the industry.[2−7] Compared with the various limitations of physical measurement instruments, deep-learning-based soft measurement technology of combustion oxygen content is becoming a hot topic for researchers. The input data to the soft sensors in refs 8−10 are the process variables of the combustion system. This requires the construction of data sets by combining measurements from multiple sensors.

Several studies[11−13] have shown that valuable information about the current combustion process can be presented from flame images taken online. This provides a new idea for combustion oxygen content measurement, that is, designing soft sensors based on flame images. A deep belief network was conducted in ref 1 to extract important features from flame images. Furthermore, the oxygen content was estimated. A more efficient method to acquire oxygen content directly from the images was proposed.[14] The high accuracy of the estimation relies on the high quality of the flame image sets, especially the high coverage of the combustion conditions as well as the uniform distribution. In practice, flame images under special combustion conditions are scarce and need to be captured by conducting specialized experiments, which is costly.

Generative adversarial networks (GANs)[15−19] show promising performance in generating images. The outstanding applications include satellite image sequence prediction,[20] dose prediction in radiotherapy,[21] and a purified terephthalic acid solvent system.[22] In the field of combustion flames, a conditional GAN was used in ref 23 to predict a two-dimensional soot signal. A hybrid model based on visual information from RGB images was proposed in ref 24 for flashover prediction. One highlight is that the dual-attention

Received: July 31, 2023
Accepted: October 5, 2023
Published: October 19, 2023

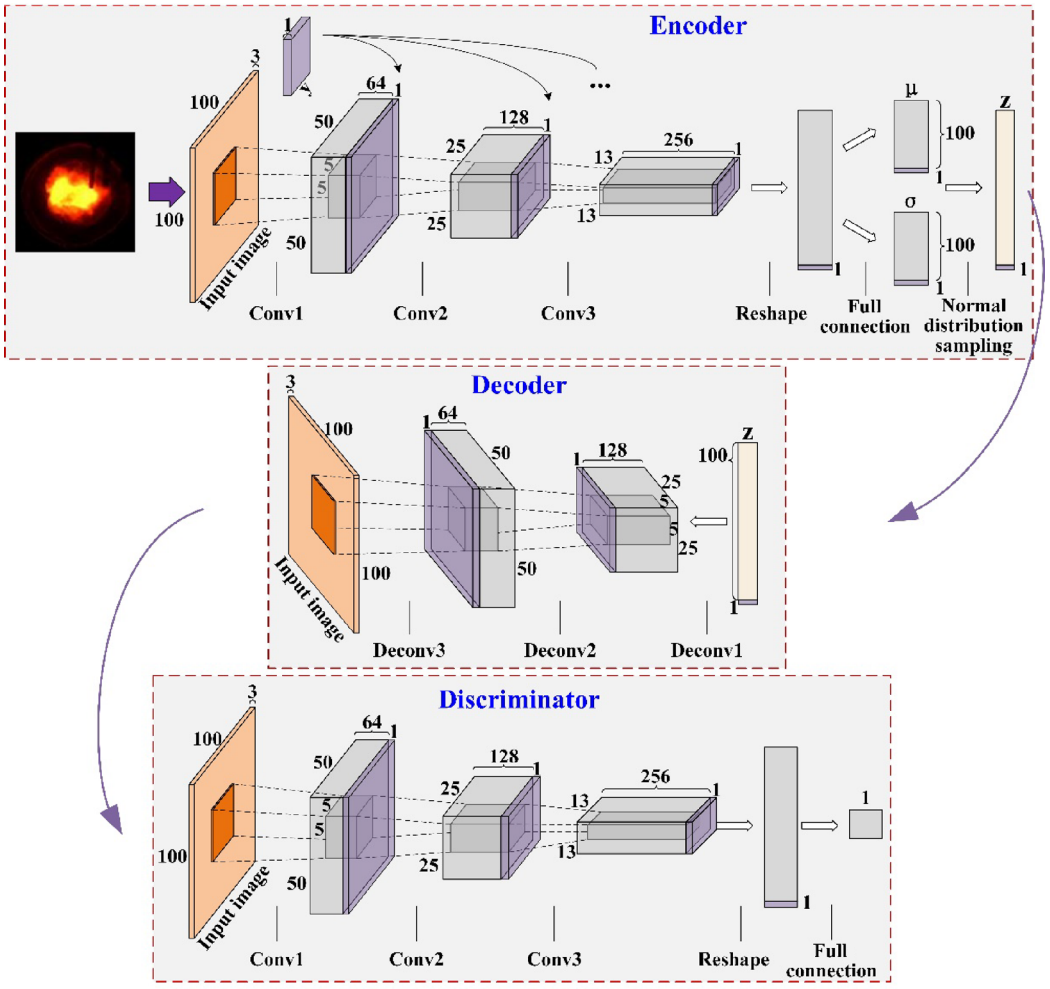

Figure 1. Structure of VA-WGAN.

GAN is developed to convert the image information into indoor temperature information. A regression GAN with gradient penalty (RGAN-GP) was presented in ref 14 for the imbalanced image-based soft sensing. The continuously changing features of labeled samples place higher demands on the performance of flame image generation models.

Autoencoder is a commonly used feature extraction technique that can compress input data into potential vectors through an encoder and learn its features. To improve the performance of the original Autoencoder, several variants have been proposed, such as sparse Autoencoder,[25] denoising Autoencoder,[26] and variational Autoencoder (VAE).[27] The denoising Autoencoder network was trained in ref 28 to extract important features of flame images. On this basis, different combustion states in the furnace are predicted. VAE can be used as a generative model because it greatly guarantees the quality of its reconstructed data.[27] VAE-GAN, which combines the characteristics of VAE and GAN, can generate more realistic samples after adversarial training.[29] Wasserstein GAN with gradient penalty (WGAN-GP) was combined with VAE to obtain VA-WGAN, which can supplement high-quality samples for the established soft sensor model.[30]

Here, a method integrating Wasserstein loss-based Generative models and a Convolutional neural network (CNN) for online Estimation (WGCE) is proposed. The innovative points are as follows:

1. A WGCE method consisting of VA-WGAN and CNN is presented for oxygen content estimation. High-precision estimation performance of the WGCE can still be guaranteed under imbalanced data sets.
2. The designed VA-WGAN can better capture information on flame images with different oxygen content values, thus providing more realistic samples for minority intervals and completing the data set enhancement.
3. The designed CNN model can estimate the combustion oxygen concentration accurately directly from flame images.

2. PROPOSED METHOD

The proposed WGCE for imbalanced flame image oxygen content estimation consists of two parts: a VA-WGAN model for data augmentation and a CNN regression model for oxygen content estimation.

2.1. VA-WGAN Data Augmentation. To generate high-quality flame images, the VA-WGAN model is given in Figure 1. The structure and parameters of VA-WGAN are shown in Table 1. Both the encoder and discriminator have three convolutional layers and one fully connected layer. The decoder contains three deconvolution layers. For all convolutional and deconvolution layers, the convolution kernel size is 5. The step size is set to 2. Leaky-ReLU, ReLU, and Leaky-ReLU are selected as the activation functions of the hidden layers of the encoder, decoder,

https://doi.org/10.1021/acsomega.3c05593
ACS Omega 2023, 8, 40657−40664

Table 1. Structure and Parameters of the VA-WGAN

composition	encoder	decoder	discriminator
structure	three convolutional layers and one fully connected layer	three deconvolution layers	three convolutional layers and one fully connected layer
activation function	Leaky-ReLU	ReLU	Leaky-ReLU
normalization	layer	batch	layer
learning rate	0.0002		
epochs	5000		
optimizer	Adam		
step size	2		
convolution kernel size	5		

and discriminator, respectively. The encoder and discriminator use the layer normalization standardization method, while the decoder uses the batch normalization standardization method. The condition variable y is expanded to a vector with size $W \times H \times 1$ and embedded into every layer of the VA-WGAN model, except for the input layer. W and H represent the width and length of the embedded feature layer, respectively.

The loss functions of the VA-WGAN can be calculated as follows:

$$L_{\mathrm{VAE}} = KL(q((z|x)|y)\|p(z|y)) - E_{q(z|x)}[\log p((x|z)|y)] \tag{1}$$

$$L_{\mathrm{WGAN}} = (E_{x_g \sim P_g}[f(x_g|y)] - E_{x_r \sim P_r}[f(x_r|y)]) + (E_{x_p \sim P_k}[f(x_p|y)] - E_{x_r \sim P_r}[f(x_r|y)]) - \lambda E_{\hat{x} \sim P_{\hat{x}}}[(\|\nabla_{\hat{x}} f(\hat{x}|y)\|_2 - 1)^2] \tag{2}$$

$$L_{\mathrm{VA-WGAN}} = L_{\mathrm{VAE}} + \omega L_{\mathrm{WGAN}} \tag{3}$$

where x, y, and z are the raw data, conditional variable, and latent vector, respectively. $q(z \mid x)$represents the probability distribution of $z \mid x \sim N(0,1)$. $p(z \mid y)$ denotes the true distribution of $z \mid y$. $\|$ denotes the calculation of the Kullback–Leibler divergence[31] for $q((z \mid x) \mid y)$ and $p(z \mid y)$. $x \mid z \sim N(\mu(z), \sigma(z))$. $\mu(z)$ and $\sigma(z)$ are the means and variances of the Gaussian distribution corresponding to z, respectively. E denotes the expectation. The distributions of real and generated data are denoted as P_r and P_g, respectively. x_r and x_g represent real samples and generated samples, respectively. $f()$ represents the output of the discriminator. x_p is the sample generated after random noise is input to the decoder. P_k is the sample distribution generated by passing x through the encoder and decoder. $\hat{x}$ is a linear interpolation of x_r and x_g. λ is the gradient penalty coefficient. $\|\nabla_{\hat{x}} f(\hat{x})\|_2$ is the 2-norm of the gradient. L_{VAE}, L_{WGAN}, and $L_{\mathrm{VA-WGAN}}$ are the loss functions of VAE, WGAN, and VA-WGAN, respectively. ω is the weighting factor.

The training process of VA-WGAN is given in Algorithm 1.

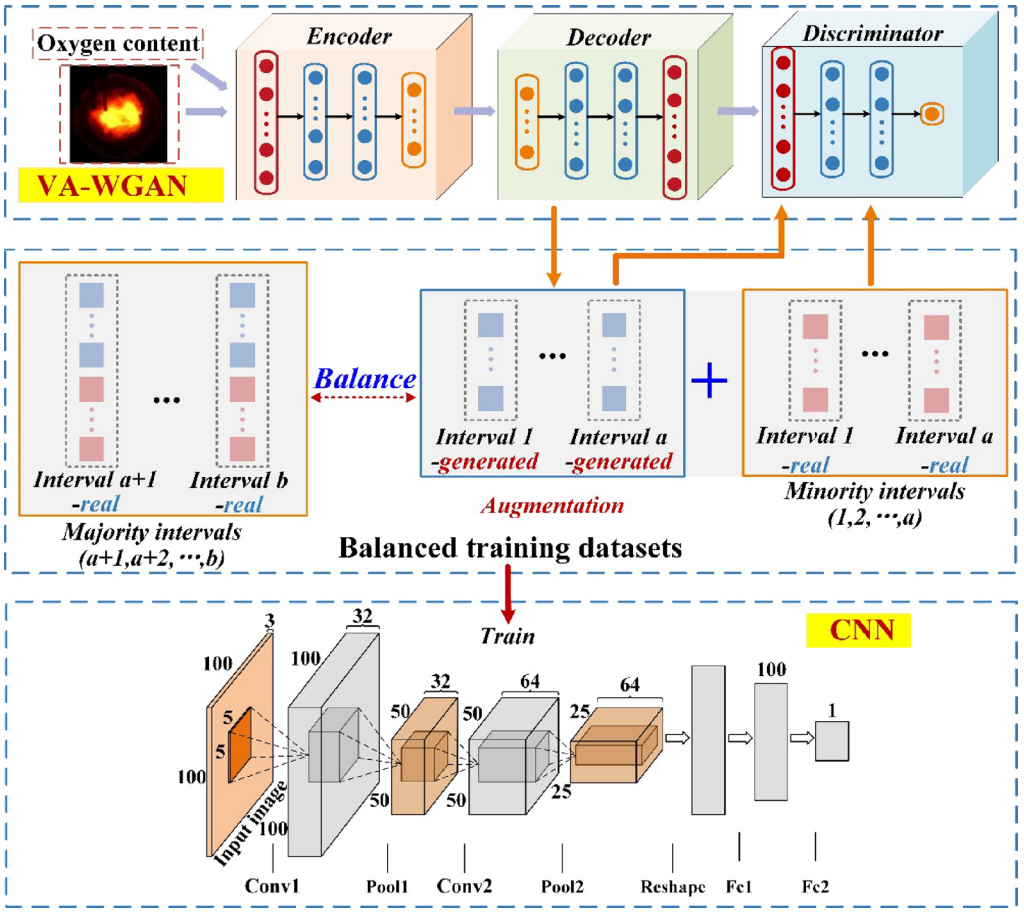

Figure 2. Designed structure for estimation of combustion oxygen content.

https://doi.org/10.1021/acsomega.3c05593
ACS Omega 2023, 8, 40657−40664

Algorithm 1. Training process of VA-WGAN

1: Sample n examples $\{x^1 \mid y^1, x^2 \mid y^2, \ldots, x^n \mid y^n\}$ from the training dataset x and condition variable y.

2: Sample n noise samples $\{\mathbf{z}_p^1, \mathbf{z}_p^2, \ldots, \mathbf{z}_p^n\}$ from a noise distribution $P_z(\mathbf{z}) \sim U[-1,1]$, and embed the conditional variable to obtain $\{\mathbf{z}_p^1 \mid y^1, \mathbf{z}_p^2 \mid y^2, \ldots, \mathbf{z}_p^n \mid y^n\}$.

3: Obtain potential variables $\{z^1 \mid y^1, z^2 \mid y^2, \ldots, z^n \mid y^n\}$, where $z^i = En(x^i \mid y^i)$, En represents the encoder.

4: Obtain generated data $\{x_g^1 \mid y^1, x_g^2 \mid y^2, \ldots, x_g^n \mid y^n\}$, where $x_g^i = De(z^i \mid y^i)$, De represents the decoder.

5: Obtain additional generated data $\{x_p^1 \mid y^1, x_p^2 \mid y^2, \ldots, x_p^n \mid y^n\}$, where $x_p^i = De(\mathbf{z}_p^i \mid y^i)$.

6: Obtain the penalty examples $\{\hat{x}^1 \mid y^1, \hat{x}^2 \mid y^2, \ldots, \hat{x}^n \mid y^n\}$, where $\hat{x}^i = a(x^i \mid y^i) + (1-a)De(z^i \mid y^i)$, $a \sim U[0,1]$.

7: Update the parameter θ_e by increasing the gradient of the encoder:

$$\nabla_v(\theta_e)1/n\sum_{i=1}^{n}\left\{KL(q((z^i \mid x^i) \mid y^i) \| p(z^i \mid y^i)) - E_{q(z^i \mid x^i)}[\log p((x^i \mid z^i) \mid y^i)]\right\}$$

8: Update the parameter θ_g by increasing the gradient of the decoder:

$$\nabla_v(\theta_g)1/n\sum_{i=1}^{n}E_{q(z^i \mid x^i)}[\log p((x^i \mid z^i) \mid y^i)] - \omega L_{WGAN}^i$$

9: Update the parameter θ_d by increasing the gradient of the discriminator:

$$\nabla_v(\theta_d)1/n\sum_{i=1}^{n}L_{WGAN}^i$$

10: **Repeat** Step1-Step9, **until** the convergence of $L_{VA-WGAN}$.

2.2. CNN-Based Regression Model. To realize the estimation of oxygen content, a CNN regression model that directly uses flame images as input is shown in Figure 2. The model has two convolutional layers, two pooling layers, and two fully connected layers. The kernel size, step size, and activation functions of the convolutional layers are 5, 1, and ReLU, respectively. The convolution kernel size of pooling layers is the same as convolutional layers, but the step size is 2. All hidden layers of fully connected layers use ReLU activation functions. Algorithm 2 presents the detailed training process.

1: Sample r examples $\{x^1 \mid y^1, x^2 \mid y^2, \ldots, x^r \mid y^r\}$ from the training dataset x and condition variable y.

2: Sample r examples $\{y_1^1, y_1^2, \ldots, y_1^r\}$ from the estimated value y_1^i.

3: Update the parameter θ_{CNN} by increasing the gradient of the CNN:

$$\nabla_v(\theta_{CNN})1/n\sum_{i=1}^{r}(y_1^i - y^i)^2$$

4: **Repeat** Step1-Step3, **until** convergence.

The designed structure for the estimation of the combustion oxygen content is given in Figure 2. The VA-WGAN is responsible for expanding the samples in minority intervals to obtain balanced data sets. Subsequently, the CNN is trained using the obtained data sets. After the training, the CNN can estimate the combustion oxygen concentration values depending on the flame images.

3. EXPERIMENTAL ARRANGEMENT

3.1. Furnace Flame Image Experimental System. The system has a 5514-6 burner, which can reach 451,000 kcal/h. The industrial heavy oil and air required for combustion come from the fuel tank and the air compressor, respectively. During combustion, the flame images are captured with a resolution of 658 × 492 pixels through an 18.5 cm-diameter window in the furnace wall. The flue gas analyzer is equipped with the ability to monitor the oxygen content in real time. The captured flame images and the oxygen content measurements are recorded by a time stamp. Figure 3 gives the composition of the entire experimental system.

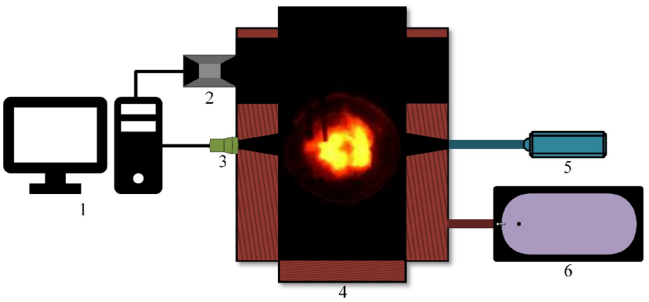

Figure 3. Furnace flame image experimental system: 1—computer, 2—flue gas analyzer, 3—camera, 4—furnace, 5—air compressor, and 6—fuel tank.

Relying on this system, 8512 flame images with oxygen concentration labels were acquired. To reduce the computational complexity, the flame images are compressed to three-channel images with 100 × 100 size. Subsequently, the data sets were grouped into 11 intervals, as shown in Table 2 according to oxygen concentration labels. For each interval, the ratio of training samples to test samples is 7:3.

Table 2. Detailed Datasets with 11 Intervals

interval	oxygen content (%)	number of samples
1	7.15−7.22	725
2	6.73−6.88	847
3	6.26−6.39	847
4	5.74−5.88	856
5	5.16−5.32	481
6	4.58−4.69	619
7	3.96−4.11	847
8	3.38−3.49	880
9	2.69−2.95	846
10	1.91−2.05	790
11	1.13−1.27	774

3.2. Scheme and Evaluation Criteria. *3.2.1. Scheme.* The designed VA-WGAN model of the WGCE is applied for the generation of samples in minority intervals, thus solving the problem of imbalanced training data sets. For the training of VA-WGAN, the learning rate and epochs are 0.0002 and 5000, respectively. Afterward, the original imbalanced data sets are expanded via the generation ability of the trained VA-WGAN. Sequently, the CNN-based regression model is trained, with the learning rate and epochs of 0.001 and 400, respectively. The Adam optimizer is used for both pieces of training. The Python codes of the proposed WGCE method are available at GitHub (https://GitHub.com/GaussG/WGCE.git).

Several recent methods, including the VAE,[27] VAE-GAN,[29] WGAN-GP,[32] and RGAN-GP,[14] are implemented to generate flame images for minority intervals and compared with the VA-WGAN. Additionally, partial least squares (PLS)[2] and support vector regression (SVR)[1] are used for oxygen content estimation and compared with the CNN regression model.

3.2.2. Evaluation Criteria. The root mean square error (RMSE), relative improvement performance (RIP), and

https://doi.org/10.1021/acsomega.3c05593
ACS Omega 2023, 8, 40657−40664

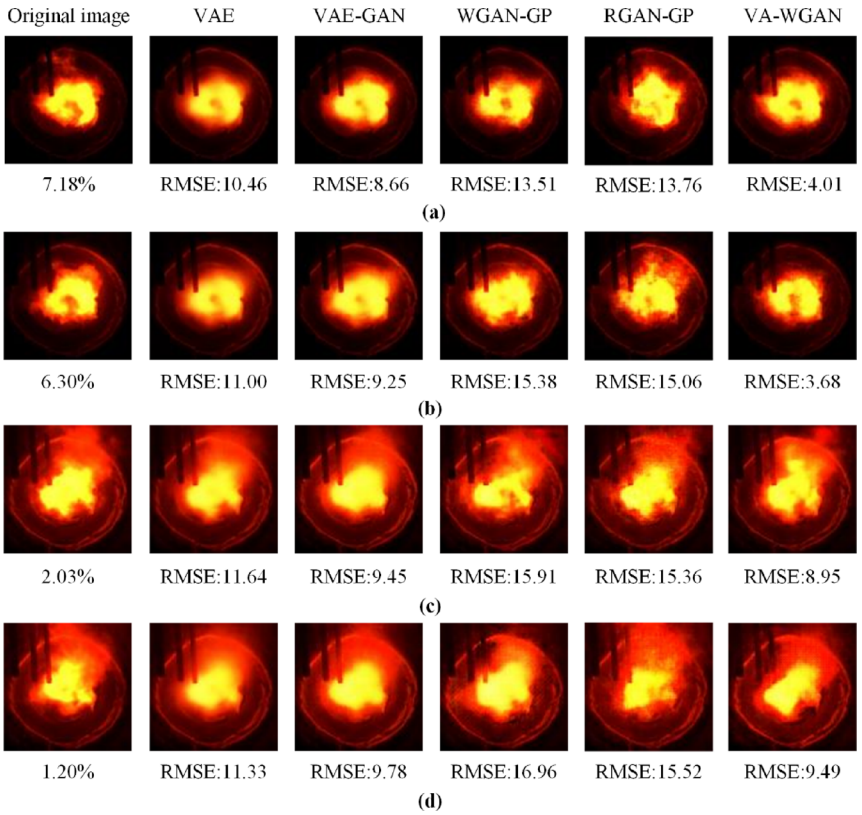

Figure 4. Comparison of images generated by different models in different intervals: (a) interval 1, (b) interval 3, (c) interval 10, and (d) interval 11.

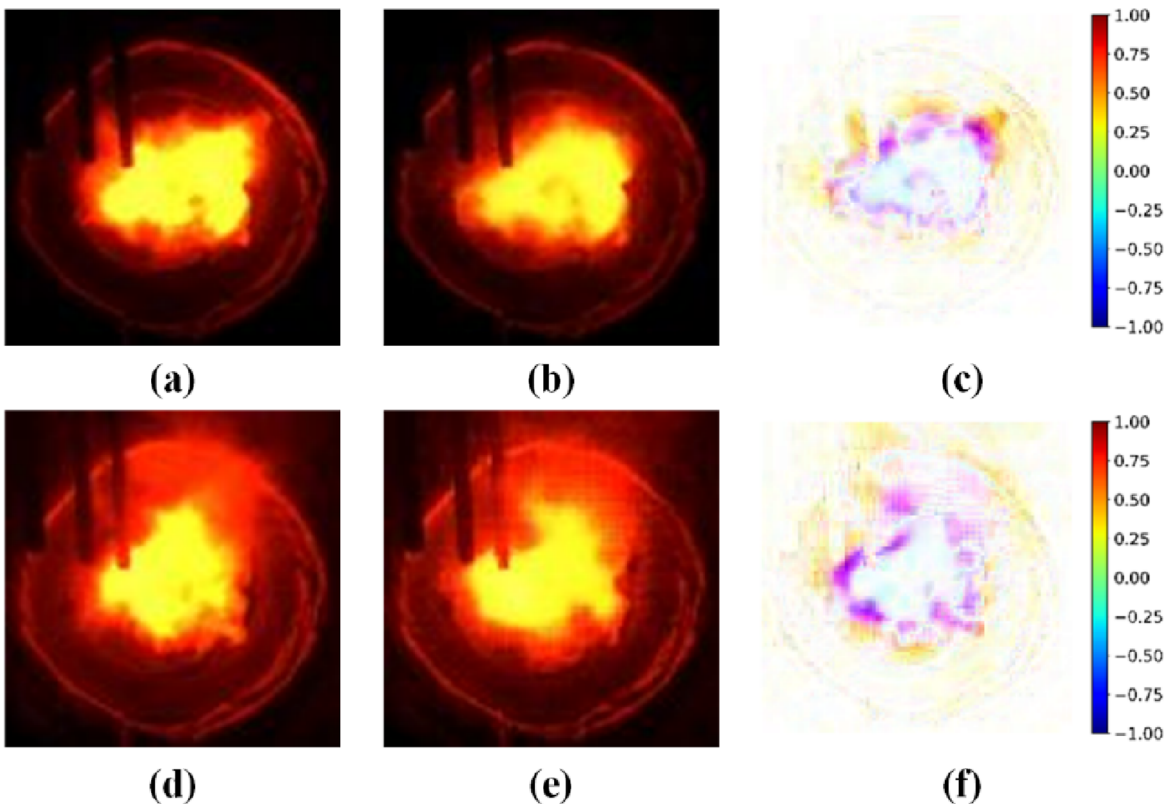

Figure 5. (a) Original, (b) VA-WGAN reconstruction, (c) error maps for interval 1, (d) original, (e) VA-WGAN reconstruction, and (f) error maps for interval 11.

coefficient of determination R^2 indices are adopted to evaluate the estimation performance. They are given as follows:

https://doi.org/10.1021/acsomega.3c05593
ACS Omega 2023, 8, 40657−40664

$$\mathrm{RMSE} = \sqrt{\frac{\sum_{i=1}^{N_t} (y_i - f(x_i))^2}{N_t}} \tag{4}$$

where $f(x_i)$ and y_i denote the estimated and real values, respectively. N_t is the number of test samples.

$$\mathrm{RIP} = \left(\frac{\mathrm{RMSE_{bef}} - \mathrm{RMSE_{aft}}}{\mathrm{RMSE_{bef}}}\right) \times 100\% \tag{5}$$

where $\mathrm{RMSE_{bef}}$ and $\mathrm{RMSE_{aft}}$ represent the RMSE values before and after the improvement, respectively.

$$R^2 = \frac{\sum_{i=1}^{N_t} (f(x_i) - \bar{y})^2}{\sum_{i=1}^{N_t} (y_i - \bar{y})^2} \tag{6}$$

where $\bar{y}$ is the mean value of y_i.

4. RESULTS AND DISCUSSION

4.1. Image Augmentation Results. The samples in intervals 1, 3, 10, and 11 are used to train each augmentation method discussed in subsection 3.2.1, respectively. As exhibited in Figure 4, compared with the original images, the reconstructed ones using these models seem similar. However, through comparison, it is found that the images generated by the VAE are blurrier. This indicates that VAE does not extract flame features well. Compared to other models, VA-WGAN has a smaller RMSE, which means that VA-WGAN produces better reconstruction results.

Moreover, the errors between the original and reconstructed images of intervals 1 and 11 are visualized, as shown in Figure 5. The lighter the color in Figure 5c,f, the smaller the reconstruction errors. Due to the insufficient oxygen supply of the inner layer during the combustion process, the combustion is relatively stable. The outer layer, in contrast, is difficult to extract features from because it burns completely and violently. It can be observed from Figure 5c,f that the inner layer reconstruction error is smaller while the outer layer is larger. This is consistent with the combustion process.

4.2. Estimation Results with Different Generation Models. To verify the performance of WGCE on oxygen content estimation under imbalanced flame images, 11 cases of imbalanced data sets are established. In each case, the number of samples in the corresponding interval in Table 2 is reduced to 60. Simultaneously, the number of samples in other intervals remains unchanged. The data set in each case is applied to train the CNN model.

To prevent the worsening of the estimation performance caused by the imbalanced data sets, VAE, VAE-GAN, WGAN-GP, RGAN-GP, and the proposed VA-WGAN are trained by the samples of minority interval in each case, respectively. After their training is complete, the corresponding minority interval is expanded by the generative model. Subsequently, the CNN model is constructed using the augmented data sets. Taking intervals 1, 3, 10, and 11 examples, the estimated results are compared in Table 3. The minority interval is denoted as MI. From the results in Table 3, the WGCE exhibits the lowest RMSE and the highest RIP. The closer R^2 is to 1, the smaller the error between the true value and the predicted value is. The R^2 values in Table 3 indicate that the proposed WGCE exhibits the highest accuracy.

For illustration, when the minority interval is 11, the oxygen content estimated by different models is as shown in Figure 6. It can be observed that the estimated points for interval 11 using CNN and VAE CNN models are far from the oxygen concentration estimation curve. This indicates that data imbalance can affect the estimated results of the oxygen content. Moreover, the VAE method did not capture the flame characteristics well. As a result, the expanded data set failed to improve the performance of oxygen content estimation. The estimation points of the VAE-GAN CNN, WGAN-GP CNN, RGAN-GP CNN, and WGCE models are all clustered around the true oxygen content curve. It means that they can better estimate the oxygen content based on imbalanced data sets. Furthermore, WGCE is the best oxygen concentration estimation method with an RMSE of 0.1103, as shown in Table 3.

Table 3. Comparison Results of Different Generative Models

MI	training data sets	method	RMSE	RIP	R^2
1	MI:60	CNN	0.1175		0.99626
	MI:60+VAE:500	VAE CNN	0.1182	−0.6300	0.99621
	MI:60+VAE-GAN:500	VAE-GAN CNN	0.1167	0.6811	0.99631
	MI:60+WGAN-GP:500	WGAN-GP CNN	0.1166	0.7066	0.99631
	MI:60+RGAN-GP:500	RGAN-GP CNN	0.1157	1.4984	0.99637
	MI:60+VA-WGAN:500	WGCE	**0.1153**	**1.8730**	**0.99640**
3	MI:60	CNN	0.1165		0.99632
	MI:60+VAE:500	VAE CNN	0.1155	0.8753	0.99638
	MI:60+VAE-GAN:500	VAE-GAN CNN	0.1128	3.1923	0.99655
	MI:60+WGAN-GP:500	WGAN-GP CNN	0.1127	3.3210	0.99656
	MI:60+RGAN-GP:500	RGAN-GP CNN	0.1132	2.8576	0.99652
	MI:60+VA-WGAN:500	WGCE	**0.1085**	**6.9167**	**0.99681**
10	MI:60	CNN	0.1252		0.99575
	MI:60+VAE:500	VAE CNN	0.1239	1.0466	0.99584
	MI:60+VAE-GAN:500	VAE-GAN CNN	0.1184	5.3927	0.99620
	MI:60+WGAN-GP:500	WGAN-GP CNN	0.1172	6.4073	0.99628
	MI:60+RGAN-GP:500	RGAN-GP CNN	0.1122	10.3619	0.99658
	MI:60+VA-WGAN:500	WGCE	**0.1111**	**11.2570**	**0.99665**
11	MI:60	CNN	0.1208		0.99604
	MI:60+VAE:500	VAE CNN	0.1200	0.6953	0.99610
	MI:60+VAE-GAN:500	VAE-GAN CNN	0.1141	5.5459	0.99647
	MI:60+WGAN-GP:500	WGAN-GP CNN	0.1133	6.1833	0.99652
	MI:60+RGAN-GP:500	RGAN-GP CNN	0.1110	8.1202	0.99666
	MI:60+VA-WGAN:500	WGCE	**0.1103**	**8.6996**	**0.99670**

4.3. Estimation Results with Different Regression Models. To further validate the superiority of the WGCE model, PLS and SVR are introduced to compare with the CNN regression model in WGCE. To create two imbalance conditions, the number of samples in intervals 1 and 11 was reduced to 60, respectively. Subsequently, the imbalanced data sets were used to train the CNN, PLS, and SVR, respectively.

Next, the two minority intervals were expanded with the VA-WGAN model. After the expansion, two augmented data sets were obtained. Then, CNN, PLS, and SVR were trained by the

https://doi.org/10.1021/acsomega.3c05593
ACS Omega 2023, 8, 40657−40664

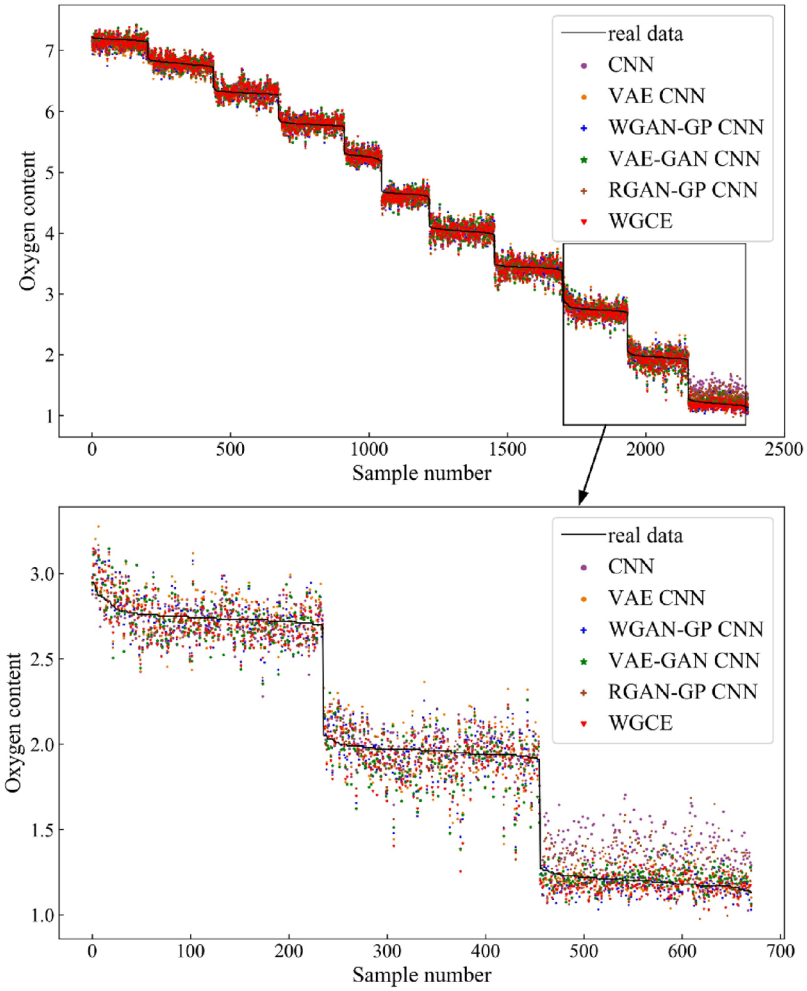

Figure 6. Comparison of estimated oxygen concentrations from different models: CNN means that the estimation is only based on the CNN model; VAE CNN, WGAN-GP CNN, VAE-GAN CNN, RGAN-GP CNN, and WGCE represent that the data sets are expanded by VAE, WGAN-GP, VAE-GAN, RGAN-GP, and VA-WGAN, respectively, before estimation of the CNN model.

augmented data sets. Detailed comparison results are given in Table 4. The designed CNN shows the best performance in estimating the combustion oxygen content among the three models. Moreover, the proposed WGCE method combined with CNN and VA-WGAN has the lowest RMSE and the highest R^2.

Table 4. Comparison Results of Different Estimation Models

MI	training data sets	model	method	RMSE	R^2
1	MI:60	CNN	CNN	0.1175	0.99626
		PLS	PLS	0.4160	0.95479
		SVR	SVR	0.4469	0.94785
	MI:60+VA-WGAN:500	CNN	WGCE	**0.1153**	**0.99640**
		PLS	VA-WGAN PLS	0.3987	0.95848
		SVR	VA-WGAN SVR	0.4225	0.95339
11	MI:60	CNN	CNN	0.1208	0.99604
		PLS	PLS	0.4321	0.95124
		SVR	SVR	0.4311	0.95147
	MI:60+VA-WGAN:500	CNN	WGCE	**0.1103**	**0.99670**
		PLS	VA-WGAN PLS	0.4143	0.95517
		SVR	VA-WGAN SVR	0.4176	0.95446

5. CONCLUSIONS

This work develops a WGCE method for combustion oxygen content estimation by incorporating a VA-WGAN data augmentation strategy and CNN regression model. The designed VA-WGAN generates virtual flame images to augment the imbalanced training data sets. In such a situation, the CNN regression model achieves a better oxygen content estimation than the PLS and SVR methods. Overall, experimental results show that the WGCE-based oxygen content estimation method with imbalanced data sets exhibits better performance than several existing methods. In the future, the WGCE model will be further explored for industrial images with large uncertainties.

AUTHOR INFORMATION

Corresponding Author

Yi Liu − *Institute of Process Equipment and Control Engineering, Zhejiang University of Technology, Hangzhou 310023, People's Republic of China;* orcid.org/0000-0002-4066-689X; Email: yliuzju@zjut.edu.cn

https://doi.org/10.1021/acsomega.3c05593
ACS Omega 2023, 8, 40657−40664

Authors

Shuang Gao − *School of Mechanical and Electrical Engineering, Shaoxing University, Shaoxing 312000, People's Republic of China*

Angpeng Liu − *Institute of Process Equipment and Control Engineering, Zhejiang University of Technology, Hangzhou 310023, People's Republic of China*

Yuxin Jiang − *Institute of Process Equipment and Control Engineering, Zhejiang University of Technology, Hangzhou 310023, People's Republic of China*

Complete contact information is available at: https://pubs.acs.org/10.1021/acsomega.3c05593

Notes

The authors declare no competing financial interest.

■ ACKNOWLEDGMENTS

The authors acknowledge the National Natural Science Foundation of China (Grant No. 62022073) and the Natural Science Foundation of Zhejiang Province (Grant No. LQ22E090007).

■ REFERENCES

(1) Liu, Y.; Fan, Y.; Chen, J. Flame images for oxygen content prediction of combustion systems using DBN. *Energy Fuels* **2017**, *31*, 8776−8783.

(2) Lin, B.; Jørgensen, S. B. Soft sensor design by multivariate fusion of image features and process measurements. *J. Process Control* **2011**, *21*, 547−553.

(3) Yoon, S.; Lee, H. W.; Liu, J. J. Quality characterization and classification of engineered stone countertops using a soft-sensor based on image analysis. *Ind. Eng. Chem. Res.* **2013**, *52*, 12337−12345.

(4) Liu, J.; Tang, Z.; Gui, W.; Liu, W.; Xu, P.; Zhu, J. Application of statistical modeling of image spatial structures to automated visual inspection of product quality. *J. Process Control* **2016**, *44*, 23−40.

(5) Smart, J.; Lu, G.; Yan, Y.; Riley, G. Characterisation of an oxy-coal flame through digital imaging. *Combust. Flame* **2010**, *157*, 1132−1139.

(6) Dai, Y.; Yang, C.; Liu, Y.; Yao, Y. Latent-enhanced variational adversarial active learning assisted soft sensor. *IEEE Sens. J.* **2023**, *23*, 15762−15772.

(7) Liu, Y.; Wang, F.; Liu, K.; Mostacci, M.; Yao, Y.; Sfarra, S. Deep convolutional autoencoder thermography for artwork defect detection. *Quant. InfraRed Thermogr. J.* **2023**, 1.

(8) Kurniawan, E. D.; Effendy, N.; Arif, A.; Dwiantoro, K.; Muddin, N. Soft sensor for the prediction of oxygen content in boiler flue gas using neural networks and extreme gradient boosting. *Neural Comput. Appl.* **2023**, *35*, 345−352.

(9) Sembodo, S. N.; Effendy, N.; Dwiantoro, K.; Muddin, N. Radial basis network estimator of oxygen content in the flue gas of debutanizer reboiler. *Int. J. Electr. Comput. Eng.* **2022**, *12*, 3044−3050.

(10) Sun, J.; Meng, X.; Qiao, J. Prediction of oxygen content using weighted PCA and improved LSTM network in MSWI process. *IEEE Trans. Instrum. Meas.* **2021**, *70*, 1.

(11) Chen, J.; Chan, L. L. T.; Cheng, Y. C. Gaussian process regression based optimal design of combustion systems using flame images. *Appl. Energy* **2013**, *111*, 153−160.

(12) Golgiyaz, S.; Talu, M. F.; Onat, C. Artificial neural network regression model to predict flue gas temperature and emissions with the spectral norm of flame image. *Fuel* **2019**, *255*, No. 115827.

(13) Onat, C.; Daşkin, M.; Toraman, S.; Golgiyaz, S.; Talu, M. F. Prediction of combustion states from flame image in a domestic coal burner. *Meas. Science and Technol.* **2021**, *32*, No. 075403.

(14) Gao, S.; Dai, Y.; Li, Y.; Jiang, Y.; Liu, Y. Augmented flame image soft sensor for combustion oxygen content prediction. *Meas. Sci. Technol.* **2023**, *34*, No. 015401.

(15) Goodfellow, I. J.; Pouget-Abadie, J.; Mirza, M.; Xu, B.; Warde-Farley, D.; Ozair, S.; Courville, A.; Bengio, Y. Generative adversarial nets. *Adv. Neural Info. Process. Syst.* **2014**, 2672−2680.

(16) Liu, K.; Li, Y.; Yang, J.; Liu, Y.; Yao, Y. Generative principal component thermography for enhanced defect detection and analysis. *IEEE Trans. Instrum. Meas.* **2020**, *69*, 1−8269.

(17) Li, J.; He, H.; Li, L. CGAN-MBL for reliability assessment with imbalanced transmission gear data. *IEEE Trans. Instrum. Meas.* **2019**, *68*, 3173−3183.

(18) Douzas, G.; Bacao, F. Effective data generation for imbalanced learning using conditional generative adversarial networks. *Expert Syst. Appl.* **2018**, *91*, 464−471.

(19) Zhu, Q. X.; Xu, T. x.; Xu, Y.; He, Y. L. Improved virtual sample generation method using enhanced conditional generative adversarial networks with cycle structures for soft sensors with limited data. *Ind. Eng. Chem. Res.* **2022**, *61*, 530−540.

(20) Dai, K.; Li, X.; Ye, Y.; Feng, S.; Qin, D.; Ye, R. MSTCGAN: multiscale time conditional generative adversarial network for long-term satellite image sequence prediction. *IEEE Trans. Geosci. Remote Sens* **2022**, *60*, 1.

(21) Zhan, B.; Xiao, J.; Cao, C.; Peng, X.; Zu, C.; Zhou, J.; Wang, Y. Multi-constraint generative adversarial network for dose prediction in radiotherapy. *Med. Image Anal.* **2022**, *77*, No. 102339.

(22) He, Y. L.; Li, X. Y.; Ma, J. H.; Lu, S.; Zhu, Q. X. A novel virtual sample generation method based on a modified conditional Wasserstein GAN to address the small sample size problem in soft sensing. *J. Process Control* **2022**, *113*, 18−28.

(23) Cheng, X.; Ren, F.; Gao, Z.; Wang, L.; Zhu, L.; Huang, Z. Predicting 3D distribution of soot particle from luminosity of turbulent flame based on conditional-generative adversarial networks. *Combust. Flame* **2023**, *247*, No. 112489.

(24) Li, Y.; Ko, Y.; Lee, W. RGB image-based hybrid model for automatic prediction of flashover in compartment fires. *Fire Saf. J.* **2022**, *132*, No. 103629.

(25) He, Y. L.; Li, K.; Zhang, N.; Xu, Y.; Zhu, Q. X. Fault diagnosis using improved discrimination locality preserving projections integrated with sparse autoencoder. *IEEE Trans. Instrum. Meas.* **2021**, *70*, 1.

(26) Li, J.; Struzik, Z.; Zhang, L.; Cichocki, A. Feature learning from incomplete EEG with denoising autoencoder. *Neurocomputing* **2015**, *165*, 23−31.

(27) Guo, F.; Bai, W.; Huang, B. Output-relevant variational autoencoder for just-in-time soft sensor modeling with missing data. *J. Process Control* **2020**, *92*, 90−97.

(28) Han, Z.; Li, J.; Zhang, B.; Hossain, M.; Xu, C. Prediction of combustion state through a semi-supervised learning model and flame imaging. *Fuel* **2021**, *289*, No. 119745.

(29) Larsen, A.; Sønderby, S. K.; Larochelle, H.; Winther, O. Autoencoding beyond pixels using a learned similarity metric. *Int. Conf. Machine Learning* **2016**, 1558−1566.

(30) Wang, X.; Liu, H. Data supplement for a soft sensor using a new generative model based on a variational autoencoder and Wasserstein GAN. *J. Process Control* **2020**, *85*, 91−99.

(31) Pu, Y.; Wang, W.; Henao, R.; Chen, L.; Gan, Z.; Li, C.; Carin, L. Adversarial symmetric variational autoencoder. *Adv. Neural Info. Process. Syst.* **2017**.

(32) Yang, W.; Xiao, Y.; Shen, H.; Wang, Z. An effective data enhancement method of deep learning for small weld data defect identification. *Measurement* **2023**, *206*, No. 112245.